A phase field study of strain energy effects on solute–grain boundary interactions

Tae Wook Heo [*], Saswata Bhattacharyya, Long-Qing Chen

Department of Materials Science and Engineering, The Pennsylvania State University, University Park, PA 16802, USA

Abstract

We have studied strain-induced solute segregation at a grain boundary and the solute drag effect on boundary migration using a phase field model integrating grain boundary segregation and grain structure evolution. The elastic strain energy of a solid solution due to the atomic size mismatch and the coherency elastic strain energy caused by the inhomogeneity of the composition distribution are obtained using Khachaturyan's microelasticity theory. Strain-induced grain boundary segregation at a static planar boundary is studied numerically and the equilibrium segregation composition profiles are validated using analytical solutions. We then systematically studied the effect of misfit strain on grain boundary migration with solute drag. Our theoretical analysis based on Cahn's analytical theory shows that enhancement of the drag force with increasing atomic size mismatch stems from both an increase in grain boundary segregation due to the strain energy reduction and misfit strain relaxation near the grain boundary. The results were analyzed based on a theoretical analysis in terms of elastic and chemical drag forces. The optimum condition for solute diffusivity to maximize the drag force under a given driving force was identified.
© 2011 Acta Materialia Inc. Published by Elsevier Ltd. All rights reserved.

Keywords: Grain boundary segregation; Solute drag effect; Elastic strain energy; Phase field model

1. Introduction

Grain boundaries are planar defects separating regions of different crystallographic orientations in a polycrystalline material and are associated with excess free energy. The interaction between grain boundaries and impurity solute atoms often leads to an inhomogeneous distribution of solute atoms near the grain boundaries, i.e. grain boundary segregation. The segregated solute atoms exert a drag force on the moving grain boundaries and thereby lower their rate of migration during grain growth or recrystallization [1,2]. Moreover, grain boundary segregation may have a pronounced effect on the mechanical properties of a material [3–8], and microstructures can be tailored for specific properties by controlling the amount of segregation. For example, in nanocrystalline materials solute segrega-

tion significantly lowers the grain boundary energy to almost zero and inhibits grain coarsening [9–12]. Therefore, a fundamental understanding of solute segregation behavior and its effects on grain boundary migration is important in designing microstructures of engineering materials with specific mechanical properties.

Grain boundary segregation has been extensively studied both experimentally and theoretically (for comprehensive reviews see Johnson [13], Seah [14], Wynblatt [15], Tingdong and Buyuan [16], Wynblatt and Chatain [17], and Lejcek and Hofmann [18]). Recent experimental studies include surface analysis techniques such as Auger electron spectroscopy (AES) and X-ray photoelectron spectroscopy (XPS) to quantitatively measure the nature and concentration of segregated species [14]. Microscopic methods with high spatial resolution (e.g. scanning transmission electron microscopy (STEM) and atom probe field ion microscopy) have also been employed [14]. However, it is still challenging to quantify grain boundary segregation

---

* Corresponding author.
E-mail address: tuh134@psu.edu (T.W. Heo).

experimentally due to the complicated interplay among energetics associated with it, such as the chemical potential of solutes, the elastic strain energy, the grain boundary energy, etc. Therefore, there have been a number of analytical models and computer simulations of grain boundary segregation [17,19–27].

The interaction between migrating grain boundaries and solute segregation, known as the solute drag effect, has also been extensively investigated [28]. Even a minute quantity of segregated impurity atoms can significantly change the grain growth kinetics during recrystallization. Solute drag can be simply considered as a coupled process of grain boundary segregation and grain boundary motion. However, the physics underlying the drag effect are not so simple. Solute segregation to a migrating grain boundary is a non-equilibrium phenomenon, and the composition profile across the moving grain boundary is usually asymmetrical due to the boundary migration. In addition, solute drag is influenced by several factors, such as grain boundary migration rate, diffusivity of solute atoms, size difference between solute and host atoms, etc. The complicated interplay among these factors hampers the quantitative and systematic experimental study of solute drag effects on the kinetics of grain boundary migration and grain growth. Therefore, theoretical models have been developed to understand the solute drag effect both qualitatively and quantitatively. The first quantitative theoretical study was conducted by Lücke and Detert [2]. They pointed out the elastic nature of the solute drag effect due to the size difference between solute and host atoms. The most successful solute drag theory was established by Cahn [1]. He described the drag effect by employing a generic interaction potential, and demonstrated two distinct velocity regimes: low and high. As a result, the grain boundary migration rate varies nonlinearly with the driving force for boundary motion. A grain boundary experiences a drag force within the low velocity regime, while it breaks away from the segregated solutes in the high velocity regime. Lücke and Stüwe extended Cahn's work and developed a simple atomistic model [29]. Hillert and Sundman further generalized the solute drag theory for systems with a high solute content. Their theory is based on the numerical calculation of free energy dissipation by solute diffusion [30]. Hillert also showed that the free energy dissipation analysis becomes identical to Cahn's impurity drag theory for grain boundary migration in dilute solutions [31,32]. A comprehensive review of these approaches is given in Hillert [33]. The effect of non-ideality on the solute drag force was also discussed by employing the regular solution model [34].

A number of attempts have been made to develop quantitative models for the solute drag effect. For example, phase field models [35–40] have been developed to study the solute drag phenomenon. The first phase field study of the solute drag effect was conducted by Fan et al. [41]. They captured the drag effect by employing the phenomenological model and applied their model to the simulation of grain growth to study the effect of solutes on the growth

kinetics and grain size distribution. Cha et al. developed a phase field model to study the solute drag effect in binary alloy systems in which the grain boundary is described as a distinguishable phase from the grain interior and the segregation potential is employed in the grain boundary region [42]. Ma et al. investigated the effects of concentration gradient, spatial variation in the gradient energy coefficient and the concentration dependence of the solute-grain boundary interactions using a regular solution model [43]. They also discussed the transition of grain boundary mobility as a function of temperature. Strandlund et al. proposed a different approach in which the effective grain boundary mobility is calculated as a function of driving force and is used to simulate grain boundary migration without solving the diffusion equation [44]. Recently Grönhagen et al. developed a phase field model [45] consistent with Cahn's solute drag theory [1]. In their model the height of the double-well potential in the expression for the Gibbs free energy is concentration dependent. Kim et al. adopted Grönhagen's model for their study of the solute drag effect [46]. They combined the solute drag model with a multiphase field model [47] for grain growth and proposed a new mechanism of abnormal grain growth induced by the solute drag effect. Li et al. also applied Grönhagen's model to study the drag effects in different velocity regimes [48]. They considered the drag force at non-steady state and the effect of a spatially variable diffusion mobility.

One of the dominant driving forces for grain boundary segregation in alloy systems is the reduction in elastic strain energy due to the redistribution of solute atoms. Solute drag is also influenced by the elastic interactions, as Lücke and Detert [2] and Cahn [1] pointed out. However, most of the solute drag theories and phase field simulations employed a generic interaction potential which arbitrarily includes all interactions arising due to chemical contributions, elastic strain effects, etc. In other words, the elastic interactions of solute atoms with the grain boundary is not explicitly described in these models and simulations. Thus a quantitative analysis of the elastic strain effects on grain boundary segregation and solute drag is not possible using the existing phase field models. Since elastic interactions have a significant effect on grain boundary segregation and solute drag, it is important to address the effects of elastic strain energy on solute–grain boundary interactions.

In this paper we present a phase field model which quantitatively takes into account the effect of elastic interactions between solutes and a grain boundary. Based on the energetics associated with the elastic strain energy of the solid solution, we formulate the elastic strain energy density due to the size difference between solute and host atoms in the presence of grain boundaries. We extend the model of Grönhagen et al. [45] by additionally incorporating the effect of elastic strain energy and integrate our model with the grain structure evolution model developed by Chen et al. [49] to study the thermodynamics and kinetics of solute segregation at static or moving grain boundaries.

Our study also theoretically explores the origin of the drag force in the presence of elastic strain interactions. We perform a systematic study of the drag force as a function of atomic size difference, driving force for grain boundary migration, and diffusivity (or diffusion coefficient). In particular, the optimum condition in terms of these variables for the strongest drag force is discussed.

2. Phase field model for solute–grain boundary interactions with strain energy

2.1. Energetics

Solute segregation at a static or migrating grain boundary is a kinetic process which leads to an inhomogeneous distribution of the solute in a polycrystalline solid solution. In the diffuse interface description, the total free energy F of a compositionally and structurally inhomogeneous system is described as a function of a set of continuous phase field variables [50]. To study the behavior of segregating solutes to a grain boundary in a binary alloy system we use a conserved field $X(\vec{r}, t)$ to describe the composition of solute and a set of non-conserved order parameters $\eta_g(\vec{r}, t)$ to describe the crystallographic orientations of grains. The total free energy F of the system is given by the volume integral [35]:

$$F = \int_V \left\{ f_{inc} + \omega \cdot g(\eta_1, \eta_2, \ldots, \eta_g) + \frac{\kappa_c}{2}(\nabla X)^2 + \frac{\kappa_o}{2}\sum_g (\nabla \eta_g)^2 + e_{coh} \right\} dV, \tag{1}$$

where f_{inc} is the incoherent local free energy density of the solid solution, g is the local free energy density of the grain structure, ω is an interaction parameter which determines the height of g, κ_c and κ_o are gradient energy coefficients associated with composition X and grain order parameters η_g, respectively, and e_{coh} is the coherency elastic strain energy density arising due to compositional inhomogeneity.

The incoherent local free energy density f_{inc} of a binary system is described using a regular solution-based model. An interaction potential E is incorporated to represent the chemical interaction between the grain boundary and solute atoms following Cahn [1]. Thus the incoherent local free energy is expressed as:

$$f_{inc} = [\mu^o + RT\ln X + \Omega \cdot (1-X)^2 + E] \cdot X + [\mu_h^o + RT\ln(1-X) + \Omega X^2] \cdot (1-X). \tag{2}$$

where μ° is the chemical potential of solute atoms at standard state, μ_h° is the chemical potential of host atoms at standard state, R is the gas constant, T is the temperature, and Ω is the regular solution parameter representing the interactions between the atoms. In the present model we specify the chemical interaction potential E as $[-m \cdot \omega \cdot g(\eta_1, \eta_2, \ldots, \eta_g)]$, where m is a parameter determining the strength of the interaction. Therefore, Eq. (2) becomes:

$$f_{inc} = \mu^o X + \mu_h^o(1-X) + RT[X\ln X + (1-X)\ln(1-X)] - m \cdot \omega \cdot g \cdot X + \Omega \cdot X(1-X). \tag{3}$$

The regular solution parameter Ω in Eq. (3) determines the non-ideality of the solid solution and intrinsically contains two contributions: one from the pure chemical effect and the other from the elastic strain due to the atomic size difference (or size mismatch) between solute atoms and host atoms. Therefore, the regular solution parameter can be expressed as a sum of two contributions:

$$\Omega = \Omega_{chem} + \Omega_{elast}^{hom}, \tag{4}$$

where Ω_{chem} is the regular solution parameter associated with the pure chemical contribution, i.e. regular solution parameter of a hypothetical solid solution in which all the atoms have the same size (this representation is similar to that of Cahn [51]), and Ω_{elast}^{hom} is the regular solution parameter due to elastic strain interactions arising from the atomic size mismatch in a solid solution. Using Eqs. (4) and (3) can be expressed as:

$$f_{inc} = \mu^o X + \mu_h^o(1-X) + RT[X\ln X + (1-X)\ln(1-X)] - m \cdot \omega \cdot g \cdot X + \Omega_{chem}X(1-X) + \Omega_{elast}^{hom}X(1-X). \tag{5}$$

The last term in Eq. (5) represents the elastic strain energy due to the size difference between solute atoms and host atoms in a homogeneous solid solution. According to Khachaturyan [52] the elastic strain energy stemming from the atomic size mismatch between the solute and matrix atoms in a homogeneous solid solution is given by:

$$e_{hom} = \frac{1}{2}[C_{ijkl}\varepsilon_{ij}^m\varepsilon_{kl}^m - \langle L(\vec{n})\rangle_{\vec{n}}]X(1-X), \tag{6}$$

where C_{ijkl} is the elastic modulus, ε_{ij}^m is the misfit strain tensor, $\langle L(\vec{n})\rangle_{\vec{n}}$ represents the average of $L(\vec{n})$ over all the directions of $\vec{n}$ with $L(\vec{n}) = n_i\sigma_{ij}^0\Omega_{jk}\sigma_{kl}^0 n_l$, $\sigma_{ij}^0 = C_{ijkl}\varepsilon_{kl}^m$, $\Omega_{jk}^{-1} = C_{jikl}n_i n_l$, and n_i denotes the unit wave vector in Fourier space. We assume a dilatational strain tensor $\varepsilon_0\delta_{ij}$ for ε_{ij}^m where δ_{ij} is the Kronecker delta function and ε_0 is the composition expansion coefficient of the lattice parameter. For elastically isotropic solids the elastic strain energy density of the homogeneous solid solution in Eq. (6) reduces to Eshelby's elastic energy for an isotropic homogeneous solid solution [53]:

$$e_{hom}^{iso} = 2\mu\left(\frac{1+v}{1-v}\right)\varepsilon_0^2 X(1-X) \quad \text{(in three dimensions)}$$

$$e_{hom}^{iso} = \left(\frac{\mu}{1-v}\right)\varepsilon_0^2 X(1-X) \quad \text{(in two dimensions)}, \tag{7}$$

where μ is the shear modulus and v is the Poisson's ratio. Replacing the last term in Eq. (5) with Eq. (7), the incoherent free energy density is expressed as:

$$f_{inc} = \mu^o X + \mu_h^o(1-X) + RT[X\ln X + (1-X)\ln(1-X)] - m \cdot \omega \cdot g \cdot X + \Omega_{chem}X(1-X) + 2\mu\left(\frac{1+v}{1-v}\right)\varepsilon_0^2 X(1-X). \tag{8}$$

Therefore, the incoherent free energy is expressed by the summation of the purely chemical free energy and elastic strain energy of the homogeneous solid solution itself. A similar expression of the incoherent free energy density with the isotropic elastic modulus was used for phase field modeling of solute segregation near a dislocation [54].

When the solute atom is larger than the matrix atom the bulk of the grain is elastically strained when a solute atom is squeezed into the matrix. However, the strain is relaxed when the solute atom approaches a grain boundary due to its relatively open structure. Relaxation of the strain is one of the main driving forces for grain boundary segregation, as noted earlier. Therefore, we model the strain relaxation near the grain boundary by using position (or grain structure)-dependent atomic size mismatch, given as:

$$\varepsilon_0(\vec{r}) = \varepsilon_c \varphi(\vec{r}), \tag{9}$$

where $\varphi(\vec{r})$ is an interpolation function, which is 1 inside grains and becomes 0 at the center of a grain boundary, and ε_c is the composition expansion coefficient of the lattice parameter inside the bulk defined as $\frac{1}{a_0}\left(\frac{da}{dX}\right)$, where a_0 is the lattice parameter of a solid solution with the overall composition X_0. If the solid solution is dilute ($X_0 \ll 1$) a_0 can be approximated as the lattice parameter of a pure host material. Assuming Vegard's law, the expansion coefficient ε_c can be evaluated as:

$$\varepsilon_c = \frac{1}{a_0}\left(\frac{da}{dX}\right) = \frac{1}{a_0}\left(\frac{\Delta a}{\Delta X}\right) = \frac{1}{a_0}\left(\frac{a_s - a_0}{1}\right)$$
$$= \frac{a_s - a_0}{a_0} \cong \frac{r_s - r_0}{r_0}, \tag{10}$$

where a_s is the lattice parameter of a pure material composed of the solute species, r_s is the radius of a solute atom, and r_0 is the radius of a host atom. Thus, the composition expansion coefficient ε_c can be considered a measure of the atomic size mismatch between the solute atoms and the host atoms. The size mismatch of a solute atom inside the bulk is ε_c, and the mismatch becomes smaller near the grain boundary. The strain is assumed to be fully relaxed when a solute atom occupies the center of a grain boundary. The mathematical form of $\varphi(\vec{r})$ is:

$$\varphi(\vec{r}) = -\left(\frac{\phi - \phi_{\min}}{\phi_{\max} - \phi_{\min}}\right)^2 + 2\left(\frac{\phi - \phi_{\min}}{\phi_{\max} - \phi_{\min}}\right), \tag{11}$$

where $\phi = \sum_g \eta_g(\vec{r})^2$, $\phi_{\max}$ is the maximum value of ϕ which corresponds to the value inside the bulk, and $\phi_{\min}$ is the minimum value of ϕ which corresponds to the value at the center of a grain boundary. The properties of the function $\varphi(\vec{r})$ are: (i) $\varphi|_{\phi=\phi_{\max}} = 1$; (ii) $\varphi|_{\phi=\phi_{\min}} = 0$; (iii) $\frac{\partial \varphi}{\partial \eta}|_{\eta_g=1\text{(grain interior)}} = 0$. Property (iii) is employed to avoid an artificial change in the equilibrium value of the grain order parameters $\eta_g(\vec{r})$ due to the elastic strain energy. Taking into account the position-dependent atomic size mismatch, we rewrite e_{hom} for a solid solution with an isotropic elastic modulus using Eq. (7):

$$e_{\text{hom}} = 2\mu\left(\frac{1+v}{1-v}\right)\varepsilon_c^2 \varphi(\vec{r})^2 X(1-X) \quad \text{(in three dimensions)}$$

$$e_{\text{hom}} = \left(\frac{\mu}{1-v}\right)\varepsilon_c^2 \varphi(\vec{r})^2 X(1-X) \quad \text{(in two dimensions)}. \tag{12}$$

To calculate the total elastic strain energy of a compositionally inhomogeneous solid solution the coherency elastic strain energy (e_{coh}) arising from the compositional inhomogeneity should be included in addition to the elastic strain energy (e_{hom}) of a homogeneous solid solution itself. Since elastic relaxation is much faster than diffusional processes, the local elastic fields are obtained by solving the mechanical equilibrium equation:

$$\nabla_j \sigma_{ij} = \nabla_j [C_{ijkl} \cdot (\varepsilon_{ki}(\vec{r}) - \varepsilon_{kl}^o(\vec{r}))] = 0, \tag{13}$$

where σ_{ij} is the local elastic stress, C_{ijkl} denotes the elastic modulus tensor, $\varepsilon_{ij}(\vec{r})$ is the total strain tensor, and $\varepsilon_{ij}^o(\vec{r})$ is the stress-free strain (or eigenstrain) tensor. Thus the term $(\varepsilon_{kl}(\vec{r}) - \varepsilon_{kl}^o(\vec{r}))$ is the elastic strain tensor.

The local stress-free strain due to the compositional inhomogeneity is given by:

$$\varepsilon_{ij}^o(\vec{r}) = \delta_{ij}\varepsilon_0(X(\vec{r}) - X_0) = \varepsilon_{ij}^m(X(\vec{r}) - X_o), \tag{14}$$

where δ_{ij} is the Kronecker delta function, ε_0 is the composition expansion coefficient of the lattice parameter, ε_{ij}^m represents the misfit strain tensor, and X_0 is the overall composition of the solid solution. The structural inhomogeneity due to the presence of a grain boundary is described using the position-dependent mismatch $\varepsilon_0(\vec{r})$ defined in Eq. (9). The total strain tensor $\varepsilon_{ij}(\vec{r})$ in Eq. (13) is expressed as the sum of the homogeneous strain $\bar{\varepsilon}_{ij}$ and heterogeneous strain $\delta\varepsilon_{ij}(\vec{r})$, and the heterogeneous strain is expressed in terms of the displacement fields $u_i(\vec{r})$ as [52]:

$$\varepsilon_{ij}(\vec{r}) = \bar{\varepsilon}_{ij} + \delta\varepsilon_{ij}(\vec{r}) = \bar{\varepsilon}_{ij} + \frac{1}{2}\left(\frac{\partial u_i}{\partial r_j} + \frac{\partial u_j}{\partial r_i}\right), \tag{15}$$

where the homogeneous strain represents the macroscopic shape change of the system and is defined such that:

$$\int_V \delta\varepsilon_{ij}(\vec{r})dV = 0. \tag{16}$$

Taking into account the strain fields defined in Eqs. (14)–(16) we solve the mechanical equilibrium equation (Eq. (13)) in Fourier space and obtain the elastic displacement fields. The coherency elastic strain energy density due to the compositional inhomogeneity is defined as:

$$e_{\text{coh}} = \frac{1}{2}C_{ijkl}(\bar{\varepsilon}_{ij} + \delta\varepsilon_{ij} - \varepsilon_{ij}^o)(\bar{\varepsilon}_{kl} + \delta\varepsilon_{kl} - \varepsilon_{kl}^o),$$
$$= \frac{1}{2}C_{ijkl}\varepsilon_{ij}^{el}\varepsilon_{kl}^{el}, \tag{17}$$

where ε_{ij}^{el} denotes the elastic strain tensor, which is equal to $(\bar{\varepsilon}_{ij} + \delta\varepsilon_{ij} - \varepsilon_{ij}^o)$. If we assume the elastic modulus of the system to be homogeneous and isotropic, the coherency elastic strain energy density defined in Eq. (17) becomes:

$$e_{\text{hom}}^{\text{iso}} = 2\mu\left(\frac{1+v}{1-v}\right)\varepsilon_0^2(X-X_0)^2 \quad \text{(in three dimensions)},$$

$$e_{\text{hom}}^{\text{iso}} = \left(\frac{\mu}{1-v}\right)\varepsilon_0^2(X-X_0)^2 \quad \text{(in two dimensions)}.$$

$$\tag{18}$$

In the original model of Grönhagen et al. [45] a simple double-well type potential $\eta^2(1-\eta)^2$ is employed. Kim et al. implemented the multiphase field model [47] for grain structure evolution in a polycrystalline structure [46]. In the present model we employ the following local free energy density function for $g(\eta_1, \eta_2, \ldots \eta_g)$ in Eq. (1) based on the model in Chen and Yang [49] associated with the evolution of grain structure with multiple grain order parameters:

$$g(\eta_1, \eta_2, \ldots, \eta_g) = 0.25 + \sum_g\left(-\frac{1}{2}\eta_g^2 + \frac{1}{4}\eta_g^4\right)$$

$$+ \gamma \sum_g \sum_{g'>g}\eta_g^2\eta_{g'}^2, \tag{19}$$

where γ is the phenomenological parameter describing the interactions among the grain order parameters. A constant 0.25 is used in Eq. (19) to make the value of g equal to 0 inside the bulk so that the interaction potential ($-m \cdot \omega \cdot g$ in Eq. (8)) is zero inside the grain. It should be noted that the addition of a constant does not affect the kinetics of the grain structure evolution.

2.2. Discussion of the free energy model

In this section we critically compare our free energy model with the existing thermodynamic models of solute segregation [45]. Neglecting the gradient energy terms, the total free energy density given in Eq. (1) is given as:

$$f = f_{\text{inc}} + \omega \cdot g + e_{\text{coh}},$$

$$= \mu^o X + \mu_h^o(1-X) + RT[X\ln X + (1-X)\ln(1-X)]$$

$$+ \Omega_{\text{chem}}X(1-X) + (1-mX)\cdot\omega\cdot g(\eta_1, \eta_2, \ldots, \eta_g)$$

$$+ e_{\text{hom}} + e_{\text{coh}},$$

$$= f_{\text{chem}} + (1-mX)\cdot\omega\cdot g + e_{\text{hom}} + e_{\text{coh}}, \tag{20}$$

where $f_{\text{chem}} = \mu^o X + \mu_h^o(1-X) + RT[X\ln X + (1-X)\ln(1-X)] + \Omega_{\text{chem}}X(1-X)$. If we ignore Ω_{chem} in f_{chem} and the elastic energy components e_{hom} and e_{coh}, the expression for the local free energy density becomes identical to that of Grönhagen et al. [45], where the barrier height of the double-well potential for the evolution of grain structure is composition dependent. The driving forces for grain boundary segregation in metallic alloy systems are both chemical and elastic in nature. The sum of the first two terms $[f_{\text{chem}} + (1-mX)\cdot\omega\cdot g]$ in Eq. (20) accounts for the chemical driving force due to the chemical potential inhomogeneity caused by the grain boundary while the sum of the last two terms $[e_{\text{hom}} + e_{\text{coh}}]$ is responsible for the elastic driving force.

The coherency elastic strain energy density e_{coh} does not include the elastic strain energy density of a homogeneous solid solution itself since e_{coh} is calculated using the homogeneous solid solution as the reference system for the compositional inhomogeneity [55]. In other words, e_{hom} is the elastic strain energy density of the homogeneous solid solution itself in a local region due to atomic mismatch, and e_{coh} is the elastic strain energy density caused by the inhomogeneous fluctuations in composition. For a system with volume V without grain boundaries and assuming it to be an elastically isotropic solid solution with compositional inhomogeneity the total elastic strain energy is calculated using Eqs. (7) and (18) as discussed in Chen [55]:

$$E_{\text{total}}^{\text{iso}} = \int_V [e_{\text{hom}}^{\text{iso}} + e_{\text{coh}}^{\text{iso}}]dV,$$

$$= \int_V [2\mu\left(\tfrac{1+v}{1-v}\right)\varepsilon_0^2 X(1-X)$$

$$+ 2\mu\left(\tfrac{1+v}{1-v}\right)\varepsilon_0^2(X-X_0)^2]d^3r,$$

$$= 2\mu\left(\tfrac{1+v}{1-v}\right)\varepsilon_0^2 \cdot V \cdot X_0(1-X_0).$$

$$\tag{21}$$

Thus, without considering the effect of grain boundaries, the total elastic strain energy of a compositionally inhomogeneous system (with an average composition X_0) is identical to that of a homogeneous solid solution having the same composition, which is in accordance with the Crum theorem.

2.3. Kinetics

The temporal evolution of the composition field X is governed by the Cahn–Hilliard equation [56], and that of the non-conserved order parameters η_g by the Allen–Cahn equation [57]. Taking into consideration the free energy of the system given by Eq. (1), we obtain the kinetic equations:

$$\frac{\partial X}{\partial t} = \nabla\cdot M_c\nabla\left(\frac{\partial f_{\text{chem}}}{\partial X} - m\cdot\omega\cdot g + \frac{\partial e_{\text{hom}}}{\partial X} + \frac{\partial e_{\text{coh}}}{\partial X} - \kappa_c\nabla^2 X\right),$$

$$\tag{22}$$

$$\frac{\partial\eta_g}{\partial t} = -L\left((1-m\cdot X)\cdot\omega\cdot\frac{\partial g}{\partial\eta_g} + \frac{\partial e_{\text{hom}}}{\partial\eta_g} + \frac{\partial e_{\text{coh}}}{\partial\eta_g} - \kappa_o\nabla^2\eta_g\right),$$

$$\tag{23}$$

where M_c is the interdiffusion mobility, L is the kinetic coefficient related to grain boundary mobility, and t is time. The derivatives of e_{hom} and e_{coh} with respect to X or η_g in Eqs. (22) and (23) are obtained as follows using Eqs. (12) and (17):

$$\frac{\partial e_{\text{hom}}}{\partial X} = 2\mu\left(\tfrac{1+v}{1-v}\right)\varepsilon_c^2\varphi(\vec{r})^2(1-2X),$$

$$\frac{\partial e_{\text{coh}}}{\partial X} = -C_{ijkl}\varepsilon_{ij}^{el}\varepsilon_c\delta_{kl}\varphi(\vec{r}),$$

$$\tag{24}$$

and

$$\frac{\partial e_{\text{hom}}}{\partial \eta_g} = 2\eta_g \left(\frac{\partial e_{\text{hom}}}{\partial \phi} \right) = 4\eta_g \mu \left(\frac{1+\nu}{1-\nu} \right) \varepsilon_c^2 \frac{\partial(\varphi^2)}{\partial \phi} X(1-X),$$

$$\frac{\partial e_{\text{coh}}}{\partial \eta_g} = 2\eta_g \left(\frac{\partial e_{\text{coh}}}{\partial \phi} \right) = -2\eta_g C_{ijkl}\varepsilon_{ij}^{el}\varepsilon_c \delta_{kl}(X-X_0)\left(\frac{\partial \varphi}{\partial \phi} \right), \quad (25)$$

where $\phi = \sum_g \eta_g(\vec{r})^2$.

The interdiffusion mobility M_c in Eq. (22) can be expressed as $D / \left(\frac{\partial^2 f_{chem}}{\partial X^2} \right)$, where D is the interdiffusion coefficient and f_{chem} is the chemical free energy defined in Eq. (20). Ignoring the regular solution parameter and assuming D to be constant, the composition-dependent mobility is given as

$$M_c = \left(\frac{D}{RT} \right) \cdot X(1-X) = M_c^0 \cdot X(1-X), \quad (26)$$

where the prefactor M_c^0 is equal to D/RT. To solve the Cahn–Hilliard equation with the composition-dependent interdiffusion mobility we use the numerical technique described in Zhu et al. [58]. The governing equations (Eqs. (22) and (23)) are solved using the semi-implicit Fourier spectral method [58,59].

3. Results and discussion

First, we study the effects of strain energy on solute segregation to a static grain boundary. The equilibrium solute composition segregated at the grain boundary is compared with the corresponding analytical solution. In the subsequent simulations the grain boundary is moved by applying artificial driving forces to study the strain energy effect on solute drag in grain boundary motion. We systematically vary the magnitude of the driving force, misfit, and diffusion mobility to study their effect on solute drag. The simulations are conducted using bicrystalline systems.

3.1. Simulation parameters

An elastically isotropic system is chosen for the simulations for simplicity, although the model is applicable to general, elastically anisotropic systems. The elastic moduli of the system are taken to be $C_{11} = 118$ GPa, $C_{12} = 60$ GPa, and $C_{44} = 29$ Gpa, which are close to those of aluminum (Al), but the Zener anisotropy factor $A_z(=2C_{44}/(C_{11} - C_{12}))$ is equal to 1. The overall composition X_0 of solutes is taken as 0.01 in all simulations. The composition expansion coefficient or atomic size mismatch ε_0 ranges from 0.00 to 0.08. For example, if we consider Al (atomic radius 0.125 nm [60]) to be the host material, the atomic size mismatch of Ni (0.135 nm [60]) or Cu (0.135 nm [60]) solutes is 0.08, that of Ga (0.130 nm [60]) solutes is 0.04, and so on. The magnitude of the eigenstrain due to the atomic size mismatch is approximately equal to $\varepsilon_c X_0$, whose value is of the order of 10^{-4}. Two different sizes of computational domains were employed. The simulations of solute segregation to

Table 1
Simulation parameters.

Parameter	Value
C_{11}, C_{12}, C_{44}	118, 60, 29 GPa
X_0	0.01
ε_c	0.00–0.08
κ_o	4.0×10^{-9} J m^{-1}
κ_c	4.0×10^{-9} J m^{-1}
ω	1.14×10^9 J m^{-3}
m	5.0
μ^o	1.0×10^9 J m^{-3}
μ_h^o	1.0×10^9 J m^{-3}
M_c^o	1.7×10^{-26}–1.7×10^{-24} m^5 J^{-1} s^{-1}
L	0.36×10^{-5} m^3 J^{-1} s^{-1}
Δx	1 nm
Δt	0.56×10^{-4} s

a static grain boundary were carried out on $256\Delta x \times 256\Delta x \times 2\Delta x$ grids, where Δx is the grid size, chosen to be 1 nm. However, longer computational domains ($2048\Delta x \times 32\Delta x \times 2\Delta x$ grids) were used to study the solute drag effect on grain boundary migration. The longer domains are used to ensure steady-state motion of the grain boundary. The gradient energy coefficients κ_o and κ_c associated with the grain order parameters and composition field, respectively, are assumed to be equal and to be 4.0×10^{-9} J m^{-1}. The barrier height ω of the grain local free energy density was taken to be 1.14×10^9 J m^{-3}. The equilibrium grain boundary energy σ_{gb} is 0.82 J m^{-2} and the equilibrium grain boundary width l_{gb} is 12 nm. These values are reasonable for a generic high angle grain boundary. The parameter m describing the chemical interaction potential in Eq. (5) is chosen to be 5.0. The chemical potentials of both solute atoms (μ^o) and host atoms (μ_h^o) at standard state are assumed to be 1.0×10^9 J m^{-3}. The prefactor M_c^o of the interdiffusion mobility M_c in Eq. (26) ranges from 1.7×10^{-26} to 1.7×10^{-24} m^5 J^{-1} s^{-1}, which corresponds to an interdiffusion coefficient D of $\sim 1.0 \times 10^{-13}$–1.0×10^{-11} cm^2 s^{-1} through the relation $D = M_c^0 RT$. The kinetic coefficient L for the Allen–Cahn equation (Eq. (23)) is chosen to be 0.36×10^{-5} m^3 J^{-1} s^{-1}, and the intrinsic mobility M_0 of the grain boundary motion is calculated to be 1.76×10^{-14} m^4 J^{-1} s^{-1} using the relation $M_0 = L \cdot \kappa_o / \sigma_{gb}$ [61]. We use the temperature T (=700 K) and the molar volume V_m of Al (=10 cm^3 mol^{-1}) for unit conversion. The time step Δt for integration is taken as 0.56×10^{-4} s. The physical parameters are summarized in Table 1. The kinetic equations are solved in their dimensionless forms. The parameters are normalized by $\Delta x^* = \frac{\Delta x}{l}$, $\Delta t^* = L \cot E \cdot \Delta t$, $\omega^* = \frac{\omega}{E}$, $\mu^* = \frac{\mu}{E}$, $f^* = \frac{f}{E}$, $C_{ij}^* = \frac{C_{ij}}{E}$, $\kappa^* = \frac{\kappa}{E \cdot l^2}$, and $M_c^{0*} = \frac{M_c^0}{L \cdot l^2}$, where E is the characteristic energy (taken to be 10^9 J m^{-3}) and l is the characteristic length (taken to be 2 nm). All the simulations were conducted using periodic boundary conditions.

3.2. Strain energy effect on grain boundary segregation

Simulations were carried out on a simple bicrystal containing a flat grain boundary. The equilibrium grain structure was first prepared without solute segregation using a phase field simulation, and then the solute species was allowed to segregate to the grain boundary by solving Eqs. (22) and (23). A high diffusivity (1.0×10^{-11} cm^2 s^{-1}) of the solute was used to rapidly achieve the equilibrium state. The pure chemical part of the regular solution parameter Ω_{chem} in Eq. (8) was set to 0 for simplicity. Since there is neither curvature of the grain boundary nor an external driving force for grain boundary motion, the grain boundary remains stationary. In the simulations of grain boundary segregation the gradient energy coefficient κ_c in

Eq. (1) was set to 0, thus reducing the Cahn–Hilliard equation (Eq. (22)) to a simple diffusion equation.

We chose a particular value of the compositional expansion coefficient ($\varepsilon_c = 0.04$) to observe the change in elastic strain energy as a function of solute segregation. The solute composition at the grain boundary increases with time (see Fig. 1a). The variation in non-dimensionalized elastic strain energy density (($e_{hom} + e_{coh}/E$) across the grain boundary is shown in Fig. 1b. Elastic strain energy density inside the grains becomes relaxed with increasing solute segregation to the boundary. As a result, the total non-dimensional elastic strain energy of the entire system ($= \int_V[(e_{hom} + e_{coh})/E]dV$) decreases with time (see Fig. 1c). Thus the elastic strain energy reduction drives the solute atoms to segregate to the grain boundary.

To quantitatively examine the effect of the elastic strain energy on grain boundary segregation the solute composition at the grain boundary were monitored as a function of the atomic size mismatch (ε_c) between the solute atoms and host atoms. To compare the simulation results with the analytical solution the simulations were conducted with ε_c ranging from 0 to 0.08. Fig. 2a shows the equilibrium composition profile across the grain boundary with increasing
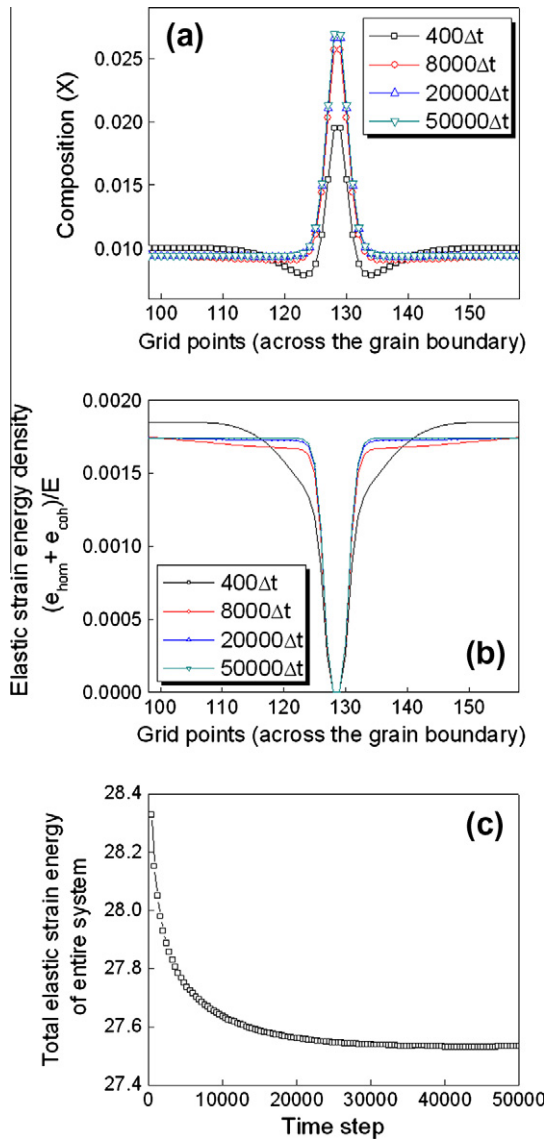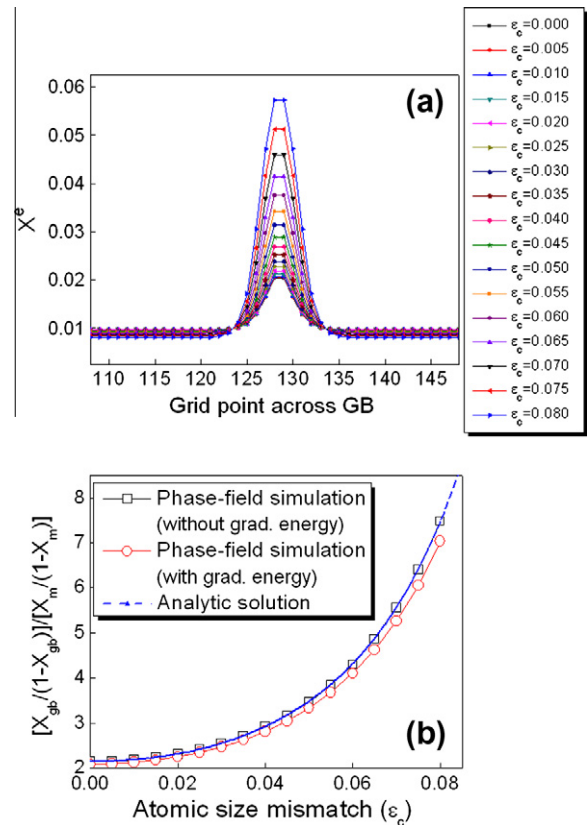

Fig. 1. Temporal evolution of (a) composition profile, (b) nondimensional elastic strain energy density across a grain boundary, and (c) nondimensional total elastic strain energy of the entire system when $\varepsilon_c = 0.04$ and $D = 1.0 \times 10^{-11}$ cm^2 s^{-1}.

Fig. 2. (a) Equilibrium composition profile near a grain boundary with atomic size mismatch (ε_c) ranging from 0.0 to 0.08 without compositional gradient energy. (b) Comparison of equilibrium solute compositions at the grain boundary as a function of atomic size mismatch obtained from phase field simulations and analytical solutions when $D = 1.0 \times 10^{-11}$ cm^2 s^{-1}.

atomic mismatch (ε_c). The concentration of segregated solute increases with increasing ε_c, since larger solute atoms prefer the grain boundary region to grain interior since the elastic strain energy can be further relaxed at the grain boundary. The analytical equation for obtaining the equilibrium solute composition at the center of the grain boundary (denoted by X_{gb}^{eq}) is given by (see Appendix A for derivation):

$$\left[\frac{X_{gb}^{eq}}{1 - X_{gb}^{eq}} \right] = \left[\frac{X_m^{eq}}{1 - X_m^{eq}} \right] \cdot \exp \left(\frac{-E_{gb} + 2\mu \left(\frac{1+\nu}{1-\nu} \right) \varepsilon_c^2 (1 - 2X_0)}{RT} \right), \quad (27)$$

where E_{gb} ($= -m \cdot \omega \cdot g_{GB}$) is the pure chemical interaction potential at the center of the grain boundary. The equilibrium solute composition at the grain boundary obtained from phase field simulations without the compositional gradient energy contribution (marked with open squares) agrees well with the corresponding analytical solution (represented by a dashed line), as shown in Fig. 2b. Solute segregation with the compositional gradient energy $\kappa_c = 4 \times 10^{-9}$ J m^{-1} was also simulated, and the degree of grain boundary segregation in this case is slightly lower than in the case without the gradient energy over the entire range of atomic mismatch.

3.3. Effect of strain energy on solute drag

3.3.1. Steady-state grain boundary migration

All prior theoretical discussions of the solute drag effect considered the steady-state motion of a grain boundary. For instance, Cahn [1] assumed a constant velocity of the migrating grain boundary to derive the drag force arising from impurities. However, almost all the previous phase field simulations have been carried out with circular grains for curvature-driven grain boundary motion during which the driving force for boundary motion increases with shrinking grain size and is not steady state. Only a few simulations [48] have considered the migration of a flat grain boundary by imposing constant velocities to achieve steady-state motion of the boundary, which should be determined before the simulations. A better evaluation of the drag forces and comparison with analytical theories can be obtained if the steady-state motion of grain boundaries is established naturally as a result of interactions among possible factors under a given driving force. Therefore, we employed a bicrystal containing a flat grain boundary to achieve steady-state grain boundary motion during a simulation. Since the flat boundary cannot move by itself, we devised an additional energy term which provides the necessary driving force for grain boundary motion, $\beta \cdot H(\eta_2)$, where β is the magnitude of the driving force for the motion and $H(\eta_2)$ is an interpolation function of grain order parameter η_2 (representing grain 2). The function H is given as $H(\eta_2) = -2\eta_2^3 + 3\eta_2^2$ and has the following properties: (i) $H(\eta_2 = 0) = 0$ and $H(\eta_2 = 1) = 1$, (ii) $\frac{dH}{d\eta_2} |_{\eta_2 = 0,1} = 0$. Property (i) of the H function allows us to assign an extra energy β only to grain 2 and property (ii)
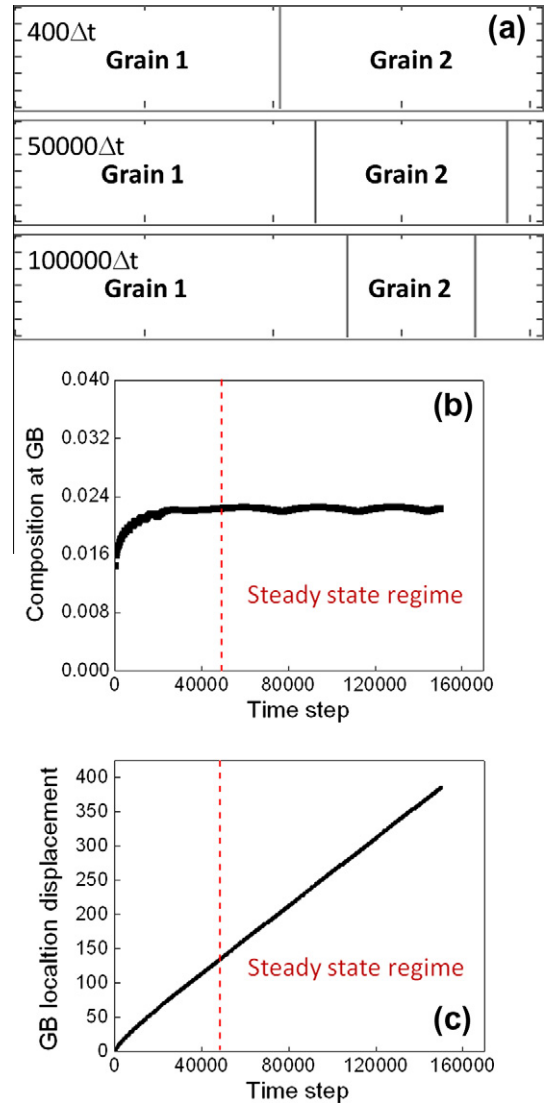

Fig. 3. (a) Migration of a flat grain boundary with periodic boundary conditions, (b) solute composition change at a grain boundary, and (c) displacement of grain boundary location as a function of time.

prevents any artificial change in the equilibrium grain order parameter values within the bulk of each grain. The energy term $\beta \cdot H(\eta_2)$ is added to the local free energy density, which is an integrand of Eq. (1). The driving force for grain boundary motion can be easily controlled by changing the magnitude of β. Thus we can plug in the driving force corresponding to the curvature of the particular grain size we are interested in. To examine the drag effect due to the presence of solute under given conditions the migrating grain boundary shown in Fig. 3a is considered. We monitored the location of the moving grain boundary and the solute composition at the grain boundary as a function of time, as shown in Fig. 3b and c, respectively. When the steady state is established the velocity of grain boundary migration is measured from the slope of the displacement–time plot using linear fitting.

3.3.2. Origin of elastic strain energy contribution to drag force: theoretical assessment

Before conducting simulations we discuss the elastic strain energy contribution to the drag force to provide a better understanding of the simulation results. Basically, the relation between the drag force P_{drag} and the driving force β is:

$$V_{gb} = M_0[\beta - P_{drag}], \tag{28}$$

where M_0 is the intrinsic mobility of the grain boundary and V_{gb} is the migration velocity. Kim et al. [46] derived the drag force from the kinetic equation assuming an instantaneous steady state with a spherical coordinate system, since they considered a spherical grain in their analysis. Using a similar procedure we derived the drag force exerted by the solute atoms on the migrating flat grain boundary under a given constant driving force in a Cartesian coordinate system. The drag force is derived as (see Appendix B for the derivation):

$$P_{drag} = m\omega \int_{-\infty}^{+\infty} X \cdot \left(\frac{\partial g}{\partial x}\right) dx$$
$$- 4(1 - 2X_0)\mu \left(\frac{1+v}{1-v}\right) \int_{-\infty}^{+\infty} X \cdot \varepsilon_0 \left(\frac{\partial \varepsilon_0}{\partial x}\right) dx, \tag{29}$$

Based on the functional form of the drag force in Eq. (29) we can easily understand that the asymmetrical distribution of solute composition across the moving grain boundary is the key to a non-zero drag force, since $\left(\frac{\partial g}{\partial x}\right)$ and $\varepsilon_0\left(\frac{\partial \varepsilon_0}{\partial x}\right)$ in the integrands are odd functions. The static grain boundary generates a symmetrical distribution of solute composition across the boundary, and the drag force is therefore equal to zero.

The first term in Eq. (29) is identical to Cahn's expression for the drag force [1] using the definition $E = -m \cdot \omega \cdot g$. One remarkable point of the derivation is the existence of the second term in Eq. (29). Both the atomic mismatch itself and its position dependency (or grain structure dependency) contribute to the second term. In other words, both the magnitude of misfit strain itself and its relaxation near a grain boundary contribute to the solute drag force. In our model we separate the interactions between the solute and grain boundary into a pure chemical interaction (E) and an elastic strain interaction. Thus the first term accounts for the drag force due to the pure chemical interaction and the second term describes the drag force due to the elastic strain interaction. The increase in atomic size mismatch inside the bulk (ε_c) would induce enhanced grain boundary segregation, similar to the equilibrium grain boundary segregation discussed above, and cause a stronger drag force due to an increase in the first term. At the same time, the increase in ε_c itself gives rise to an enhancement of the drag force stemming from the second term in Eq. (29), since $\varepsilon_0\left(\frac{\partial \varepsilon_0}{\partial x}\right)$ and $\left(\frac{\partial g}{\partial x}\right)$ have opposite signs. Therefore, the elastic strain energy contribution to the solute drag effect is significant.

Employing the Cahn–Hilliard diffusion equation (Eq. (22)), the drag force in Eq. (29) reduces to a simpler expression in terms of measurable variables such as grain boundary migration velocity at steady state and diffusivity, given as (see also Appendix B for the derivation):

$$P_{drag} = RTV_{gb} \int_{-\infty}^{+\infty} \frac{(X - X_m)}{D(1 - X)} dx, \tag{30}$$

where X_m is the solute composition inside the grain. The expression in Eq. (30) implicitly contains the contribution from elastic strain interaction, while the expression for the drag force in Eq. (29) explicitly shows the contribution from the elastic strain.

3.3.3. Solute drag under different driving forces

Evaluation of the solute drag effect under several driving forces for grain boundary motion will be useful because the magnitude of the driving force in our model for the migration of a planar grain boundary corresponds to a particular radius of a circular grain in the case of curvature-driven grain boundary motion, as noted earlier. Thus a set of simulations under different levels of the driving force for boundary motion will provide us with information regarding the stability of the grain structure in terms of an average grain size. In addition, the dependency of the drag
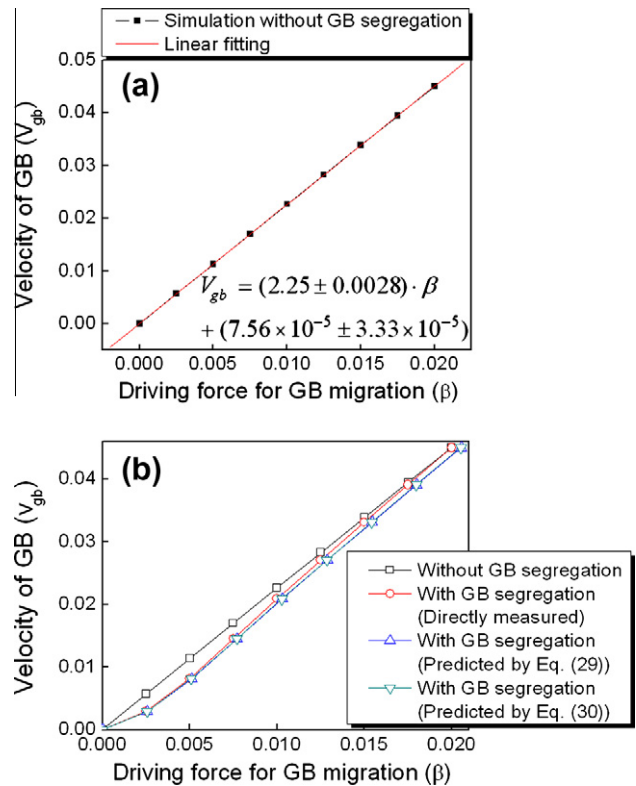

Fig. 4. (a) Grain boundary velocity as a function of driving force without solutes and its linear fitting, and (b) grain boundary migration velocity as a function of driving force with solutes of $D = 1.0 \times 10^{-12}\,\mathrm{cm^2\,s^{-1}}$ when elastic strain effects are ignored and its comparison with theoretical predictions.

force on atomic mismatch will give us guidelines for the selection of solutes to suppress grain growth.

We first conducted simulations of the solute drag effect in the absence of elastic strain energy. These simulations provide us with a benchmark with which we can compare the results of the drag effect when elastic strain interactions are taken into consideration. As a reference, grain boundary motion without solute was first simulated with a driving force varying from 0 to 0.02 in dimensionless units. The velocity of the migrating grain boundary is proportional to the driving force within this regime, as shown in Fig. 4a. The grain boundary velocity V_{gb} as a function of driving force β is fitted using the linear equation $V_{gb} = M_0 \cdot \beta$ to determine the intrinsic grain boundary mobility M_0 from the simulations. M_0 is determined to be 2.25 in dimensionless units. The value of the computationally measured intrinsic mobility is slightly (7%) smaller than the value (2.42) calculated from the equilibrium grain boundary energy σ_{gb} using the relation $M_0 = L\kappa_o/\sigma_{gb}$. This is because the migrating grain boundary is in a non-equilibrium state under this driving force.

The grain boundary motion was then simulated in the presence of solute under the same range of driving force without taking into account the elastic strain energy. The interdiffusivity D was chosen to be $1.0 \times 10^{-12} \text{ cm}^2 \text{ s}^{-1}$. As shown in Fig. 4b, the velocity of the boundary motion in this case shows a nonlinear behavior with increasing driving force, and the rate of boundary migration is slower than that of the previous case due to the solute drag effect. We compared the simulation results with the theoretical analysis by Cahn [1]. It should be noted that fully analytical calculation of the drag force under a given driving force for grain boundary motion is not an easy task, in fact almost impossible, since the velocity of grain boundary migration and the solute segregation composition are interdependent. Moreover, steady-state grain boundary motion is achieved by iterative interactions between the grain boundary velocity and the composition of the segregated solute. One possible way is to assume one of the variables for analytical calculation of the drag force. For example, we need to assume the steady-state grain boundary velocity and then calculate the composition profile across the grain boundary based on the solution of the diffusion equation for a moving grain boundary derived by Cahn [1]. With the calculated composition profile and an assumed velocity the drag force is calculated using either Eq. (29), (30). However, without information on the steady-state grain boundary velocity a pure analytical prediction of the drag force is impossible. Instead, we computed the steady-state composition profile by solving both the Cahn–Hilliard and Allen–Cahn equations under a constant driving force. It should be noted that this is the more natural way to obtain the steady-state solute composition profile near a migrating grain boundary, since the steady state is automatically achieved after iterative interactions between the solute composition profile and the migrating grain boundary by solving these well-defined equations. The drag

force is then calculated using both Eqs. (29) and (30) as a theoretical prediction in the absence of elastic interactions, i.e. only the first term is employed in the case of Eq. (29). Fig. 4b shows a comparison between the migration velocity obtained from the simulations and those estimated analytically. It should be mentioned that Eq. (30) and the first term of Eq. (29) give the same predicted results as shown in Fig. 4b in the absence of the elastic strain energy. In addition, the computationally measured velocities agree well with the theoretically predicted ones in the low driving force regime. There is a slight difference between measured and predicted velocities in the high driving force regime. The difference stems from the assumption of an equilibrium grain boundary profile (Eq. (B6)) during migration. The profile of the moving grain boundary shifts from equilibrium when the driving force is large. However, such a small discrepancy is not significant for validation of the simulations.

We next investigated the strain energy effects on solute drag and compared our results with the analytical prediction. The elastic modulus was assumed to be isotropic for simplicity. The steady-state grain boundary velocities were computationally measured under different levels of driving force for boundary motion with increasing atomic size mismatch (ε_c). To ensure the accuracy of the predictions from the simulations 136 sets of simulations (17 different values of mismatch under a particular driving force × 8 different levels of driving force) were carried out. As shown in Fig. 5a, the grain boundary velocity decreases as the mis-
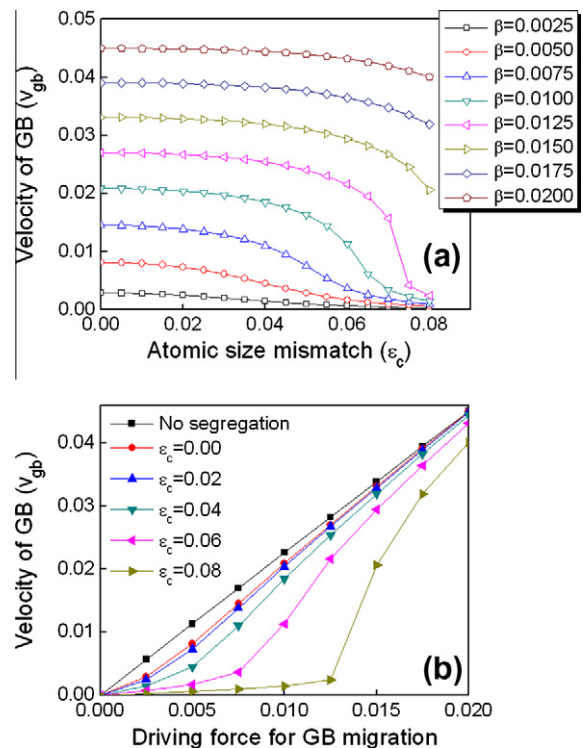

Fig. 5. (a) Grain boundary velocity with solutes with several atomic size mismatches under different driving forces with $D = 1.0 \times 10^{-12} \text{ cm}^2 \text{ s}^{-1}$, and (b) reconstructed graph with the datasets from (a).

match increases under any driving force, as expected from the discussion in Section 3.3.2. When the magnitude of the driving force is large, 0.0175 or 0.02, the grain boundary velocities are insensitive to the atomic size mismatch. Thus when the driving force is large enough the incorporation of solute atoms with large atomic radii does not effectively impede grain boundary motion. However, one can identify a critical mismatch within the range we employed in our simulations beyond which there is a sharp reduction in grain boundary velocity in the low driving force regime ($\beta < 0.0150$). For a better representation of the datasets we also plotted grain boundary velocity as a function of driving force for different levels of atomic size mismatch, shown in Fig. 5b, using the same datasets as in Fig. 5a. The plot shows the typical nonlinear behavior of a dragged grain boundary velocity with increasing driving force. The nonlinearity becomes significant with an increase in atomic mismatch, and a discontinuous change in velocity with increasing driving force becomes evident. For $\varepsilon_c = 0.08$ there is an abrupt increase in velocity when the magnitude of the driving force is above 0.0125.

As discussed earlier, both chemical and elastic interactions contribute to the drag force. We attempt to quantify each contribution based on Eq. (29) using the case of
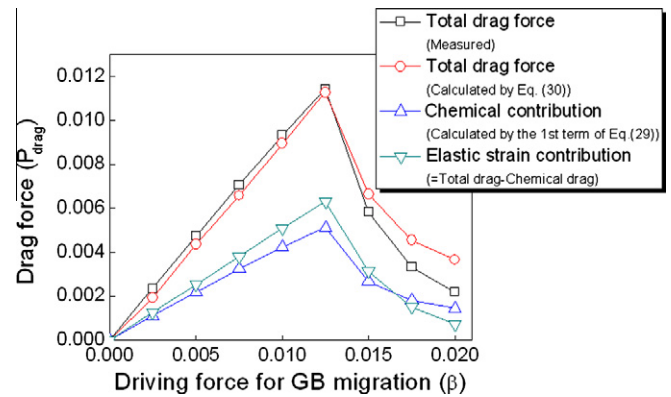

Fig. 6. Total drag force as a function of driving force for grain boundary motion. Chemical and elastic strain contributions to total drag force are plotted in the case of $\varepsilon_c = 0.08$. The solute diffusivity is assumed to be $D = 1.0 \times 10^{-12}$ cm^2 s^{-1}.

$\varepsilon_c = 0.08$ as an example. Since the intrinsic grain boundary mobility M_0, driving force β, and the grain boundary velocity are known, the total drag force can be either analytically estimated using Eq. (30) or computationally measured from the simulations using Eq. (28). The contribution from chemical interactions is calculated using
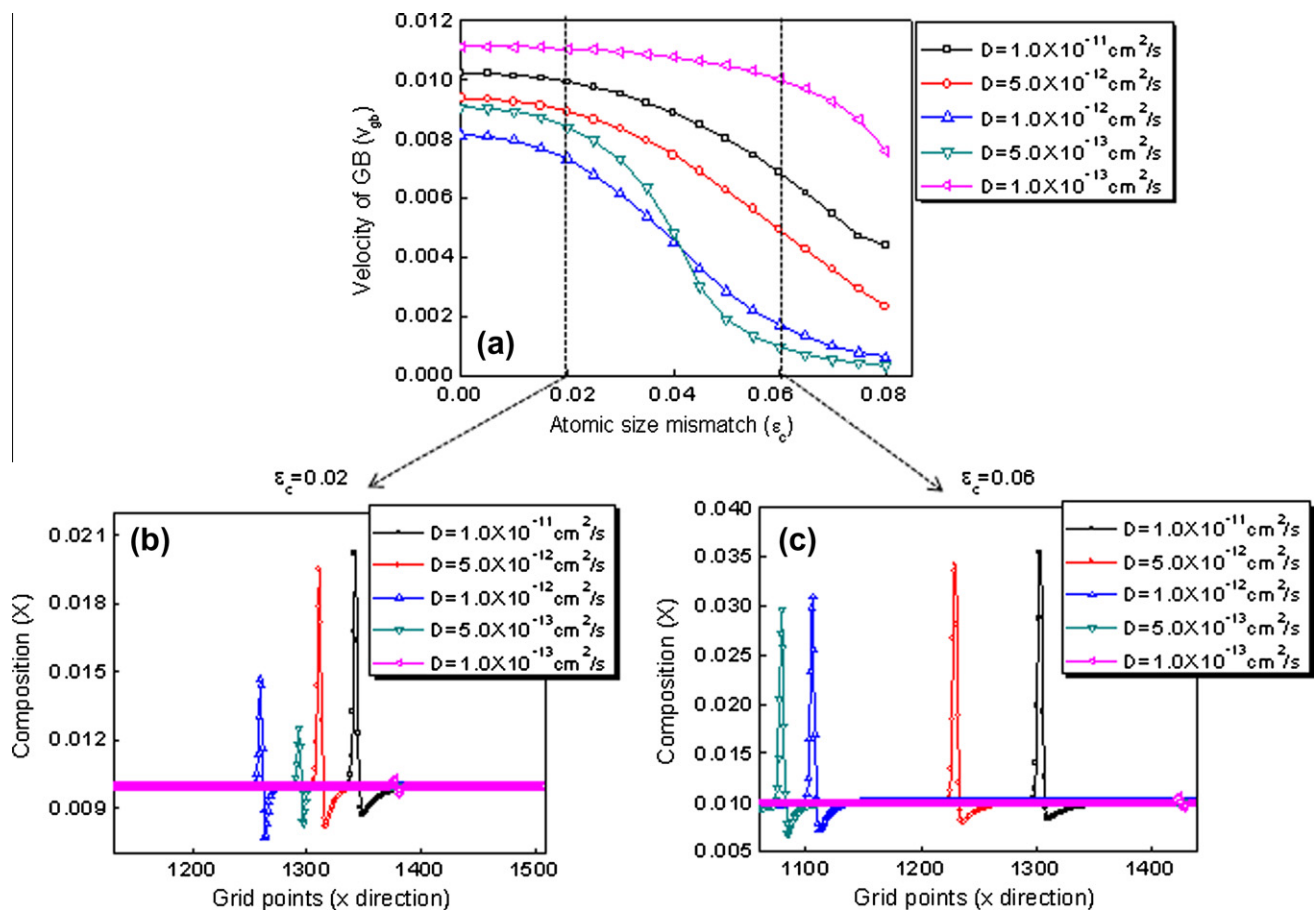

Fig. 7. (a) Grain boundary velocity for different solute diffusivities for a driving force $\beta = 0.005$, (b) composition profiles in the cases of $\varepsilon_c = 0.02$ and (c) $\varepsilon_c = 0.06$.

the first term in Eq. (29), and deducted from the measured total drag force to calculate the contribution of elastic strain. First, the computationally measured drag force agrees well with that estimated analytically using Eq. (30) (see Fig. 6). In the presence of elastic strain the drag force calculated using Eq. (30) is significantly different from the drag force calculated using the first term of Eq. (29), which shows that Eq. (30) implicitly contains the elastic strain contribution, as discussed above. We also observe that the contribution of the elastic strain interaction to the total drag force is comparable with that of the chemical interaction, in this case from Fig. 6. Based on this comparison we could confirm that the elastic strain interaction contribution to the total drag force is significant, as expected from the theoretical analysis discussed in the previous section.

3.3.4. Effect of diffusivity on solute drag

One important factor that determines the drag force is the diffusivity (or diffusion coefficient) of the solute species, as shown in Eq. (30). Solute atoms with high diffusivity can easily catch up with the migrating boundary, and the composition profile across the grain boundary can be close to a symmetrical one, i.e. an equilibrium profile. Thus solute atoms with high diffusivity will exert less drag force. On the other hand, rapidly diffusing solute atoms can easily

simultaneously segregate to a moving grain boundary. This will lead to an increase in the solute composition near the grain boundary, which, in turn, will cause an increase in the drag force. Solute atoms with low diffusivity will exhibit the opposite tendency. Therefore, we expect that there should be an optimum diffusivity of the solute which results in a maximum solute drag force in grain boundary motion. When elastic interactions are also considered the correlation between solute composition and the grain boundary migration velocity becomes more complicated. Thus it is more obvious that a computational approach is required to specify the optimum conditions for the maximum drag force.

We conducted simulations with different values of diffusivity and atomic size mismatch under a fixed driving force for grain boundary motion. The magnitudes of driving force for grain boundary motion were chosen to be 0.005 or 0.01 in dimensionless units. The diffusivities range from 1.0×10^{-13} to 1.0×10^{-11} cm^2 s^{-1}. Figs. 7a and 8a show the computationally measured velocities for different solute diffusivities as a function of mismatch when $\beta = 0.005$ and $\beta = 0.01$, respectively. In addition, the composition profiles for the cases of $\varepsilon_c = 0.02$ and $\varepsilon_c = 0.06$ when $\beta = 0.005$ are shown in Fig. 7b and c, and those for the cases of $\varepsilon_c = 0.03$ and $\varepsilon_c = 0.07$ when $\beta = 0.01$ are shown in Fig. 8b and c.
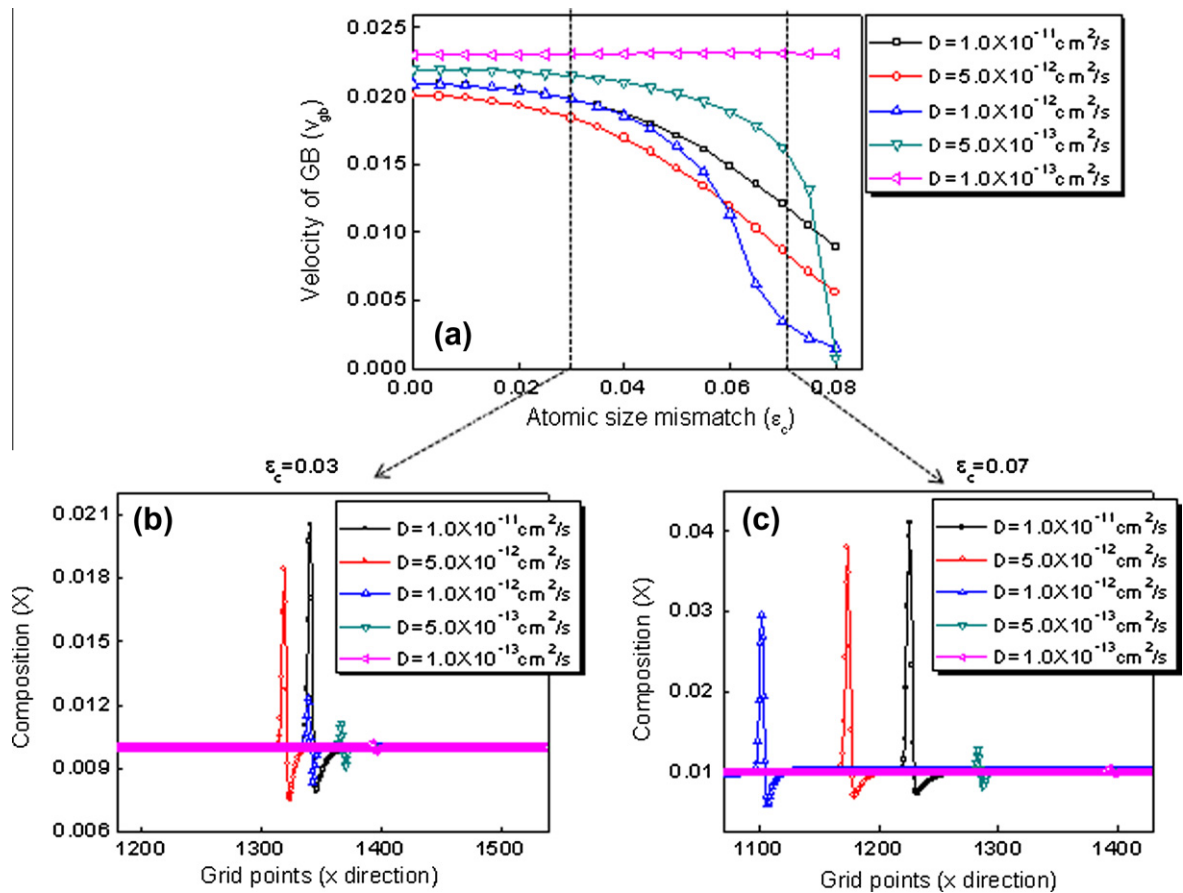

Fig. 8. (a) Grain boundary velocity for different solute diffusivities for a driving force $\beta = 0.010$, (b) composition profiles in the cases of $\varepsilon_c = 0.03$ and (c) $\varepsilon_c = 0.07$.

We observe a wide spectrum of grain boundary velocities depending on diffusivity as well as the atomic size mismatch, even though the same driving force is applied as shown in Figs. 7a and 8a. This implies that the change in either diffusivity or size mismatch is an effective way to control the grain boundary migration rate. Moreover, when the atomic size mismatch is larger, the migration velocity of the boundary is more sensitive to the solute diffusivity for both driving forces.

It should be noted that the drag force depends on a complicated interplay between the atomic size mismatch and solute diffusivity for a given driving force. In the case of the lowest diffusivity (1.0×10^{-13} cm^2 s^{-1}) very small number of solute atoms segregate to the migrating grain boundary, since few solute atoms cannot catch up with the moving boundary. The drag effect is insignificant under both driving forces ($\beta = 0.005$ and 0.01), and the dependency of the velocity on the atomic size mismatch is very slight. On the other hand, a remarkable tendency of the boundary velocity is observed (Figs. 7 and 8) as the diffusivity increases. Let us consider the case where the magnitude of the driving force $\beta = 0.005$ and the mismatch $\varepsilon_c = 0.02$ (marked by a vertical line in Fig. 7a). Under these conditions the solute with diffusivity $D = 1.0 \times 10^{-12}$ cm^2 s^{-1} results in the strongest drag force. Even though more solute atoms segregate to the grain boundary when the solute diffusivity is higher (1.0×10^{-11} and 5.0×10^{-12} cm^2 s^{-1}) the drag is less effective, since the fast diffusing solute atoms keep pace with the migrating grain boundary and the composition profile becomes more symmetrical. However, the reason for the smaller drag force when the diffusivity is low ($D = 5.0 \times 10^{-13}$ cm^2 s^{-1}) is different from the cases with high solute diffusivity. With a significantly lower solute diffusivity the relatively slow diffusion causes less solute segregation to the moving grain boundary and such a small number of solute atoms cannot effectively suppress boundary motion. When the mismatch is larger than 0.04 the optimum diffusivity for the strongest drag force is, however, different from that of the above case. The strongest drag force is achieved for $D = 5.0 \times 10^{-13}$ cm^2 s^{-1}. Even the smallest amount of solute exerts a very strong drag force within this regime, as shown in Fig. 7c. When the magnitude of the driving force is changed (e.g. $\beta = 0.01$) the optimum condition for maximum drag force changes. For example, solute atoms with a size mismatch of 0.03 suppress boundary motion most effectively when $D = 5.0 \times 10^{-12}$ cm^2 s^{-1}, but a solute with a mismatch of 0.07 gives the strongest drag force when $D = 1.0 \times 10^{-12}$ cm^2 s^{-1} (see Fig. 8a).

One interesting feature is observed in Fig. 8a and b. Significantly different amounts of solute segregation result in similar drag forces. For example, when the size mismatch is 0.03 the grain boundary velocities (as well as the drag forces) for $D = 1.0 \times 10^{-11}$ and 1.0×10^{-12} cm^2 s^{-1} are very similar to each other, although much larger numbers of solute atoms segregate to the grain boundary when $D = 1.0 \times 10^{-11}$ cm^2 s^{-1}, as shown in Fig. 8b. The faster diffusion of solute atoms enables them to easily catch up with the migrating grain boundary even though a large number of solute atoms segregate to the moving grain boundary in the case of $D = 1.0 \times 10^{-11}$ cm^2 s^{-1}. On the other hand, the small number of segregated solute atoms effectively drags the boundary migration in the case of slow diffusion ($D = 1.0 \times 10^{-12}$ cm^2 s^{-1}), since a more asymmetrical composition profile is achieved. As a result, totally different amounts of grain boundary segregation give rise to the same resultant velocities. In other words, the determining factors for the same drag forces for these two cases are different.

4. Summary

We revisited Cahn's impurity drag theory [1] with an emphasis on the contribution of the elastic strain energy to the drag force. We successfully modeled and the elastic strain energy of a polycrystalline solid solution and incorporated it into a phase field model for the quantitative study of grain boundary segregation and solute drag effects on grain boundary motion. Solute segregation to a grain boundary was simulated by taking into account the contribution of elastic strain energy, and the results compared with analytical predictions. The effect of elastic strain energy on solute drag in grain boundary motion was theoretically analyzed based on Cahn's theory. The theoretical analysis reveals that the drag force is influenced by both chemical and elastic strain interactions. The chemical interactions include the degree of grain boundary segregation as well as the asymmetry of the solute composition profile across the grain boundary. The elastic strain interaction is associated with the misfit strain relaxation near the grain boundary. We quantitatively analyzed the effects of these interactions. Our simulation results show that the grain boundary velocity depends strongly on the solute diffusivity as well as the atomic size mismatch under a given driving force for grain boundary migration. In addition, the velocity becomes more sensitive to solute diffusivity when the solute atoms have a larger size mismatch. We should emphasize that the grain boundary migration rate in the presence of solute is determined by different mechanisms under different conditions. In addition, there exists an optimum condition of solute diffusivity which results in the strongest drag effect on grain boundary motion. The optimum conditions for maximum drag force under given parameters were identified using computer simulations. It is expected that the model provides us with guidelines in terms of atomic size of solute and diffusivity to maximize the drag force and arrest grain growth in polycrystalline materials.

Appendix A: Equilibrium composition profile of grain boundary segregation

Let us consider a polycrystalline binary alloy. The binary solid solution is in thermodynamic equilibrium when $\frac{\partial f}{\partial X}(= \mu - \mu_h)$ becomes constant everywhere in the polycrystal. To determine the equilibrium composition of solute at the center of the grain boundary the following relation should be satisfied:

$$\frac{\partial f}{\partial X}\Big|_{\vec{r} \text{at GB}} = \frac{\partial f}{\partial X}\Big|_{\vec{r} \text{at Bulk}}, \tag{A1}$$

where $f = \mu^o X + \mu_h^o (1-X) + RT[X \ln X + (1-X) \ln(1-X)] + (1-mX) \cdot \omega \cdot g + e_{\text{hom}} + e_{\text{coh}}$.

Therefore,

$$\mu^o - \mu_h^o + RT \ln \frac{X_{gb}^{eq}}{1 - X_{gp}^{eq}} - m \cdot \omega \cdot g_{GB}$$

$$= \mu^o - \mu_h^o + RT \ln \frac{X_m^{eq}}{1 - X_m^{eq}} + \frac{\partial e_{\text{hom}}^{\text{bulk}}}{\partial X} + \frac{\partial e_{\text{coh}}^{\text{bulk}}}{\partial X}. \tag{A2}$$

Using the homogeneous and isotropic modulus approximation (Eqs. (12) and (18)), Eq. (A2) becomes

$$\mu^o - \mu_h^o + RT \ln \frac{X_{gb}^{eq}}{1 - X_{gb}^{eq}} - m \cdot \omega \cdot g_{GB}$$

$$= \mu^o - \mu_h^o + RT \ln \frac{X_m^{eq}}{1 - X_m^{eq}} + 2\mu\left(\frac{1+v}{1-v}\right)\varepsilon_c^2 (1 - 2X_0). \tag{A3}$$

Rearranging Eq. (A3) we obtain the analytical expression

$$\left[\frac{X_{gb}^{eq}}{1 - X_{gb}^{eq}}\right] = \left[\frac{X_m^{eq}}{1 - X_m^{eq}}\right] \cdot \exp\left(\frac{-E_{gb} + 2\mu\left(\frac{1+v}{1-v}\right)\varepsilon_c^2(1 - 2X_0)}{RT}\right). \tag{A4}$$

where E_{gb} is defined as $[-m \cdot \omega \cdot g_{GB}]$.

Appendix B: Drag force expression with D and V_{gb}

Let us consider a bicrystal consisting of grains 1 and 2. With the driving force term $(\beta \cdot H(\eta_2))$ and elastic strain energies of the isotropic elastic modulus approximation (Eqs. (12) and (18)) the Allen–Cahn relaxation equations for η_1 and η_2 in Eq. (23) become

$$\frac{\partial \eta_1}{\partial t} = -L\left(\omega(1 - mX)\frac{\partial g}{\partial \eta_1} - \kappa_o \frac{\partial^2 \eta_1}{\partial x^2}\right.$$

$$+ 4\mu\left(\frac{1+v}{1-v}\right)\varepsilon_0 \frac{\partial \varepsilon_0}{\partial \eta_1} X(1-X)$$

$$\left. + 4\mu\left(\frac{1+v}{1-v}\right)\varepsilon_0 \frac{\partial \varepsilon_0}{\partial \eta_1}(X - X_0)^2\right),$$

$$\frac{\partial \eta_2}{\partial t} = -L\left(\omega(1 - mX)\frac{\partial g}{\partial \eta_2} - \kappa_o \frac{\partial^2 \eta_2}{\partial x^2} + \beta\left(\frac{\partial H}{\partial \eta_2}\right)\right.$$

$$+ 4\mu\left(\frac{1+v}{1-v}\right)\varepsilon_0 \frac{\partial \varepsilon_0}{\partial \eta_2} X(1-X)$$

$$\left. + 4\mu\left(\frac{1+v}{1-v}\right)\varepsilon_0 \frac{\partial \varepsilon_0}{\partial \eta_2}(X - X_0)^2\right). \tag{B1}$$

If the boundary moves along the direction perpendicular to itself (x direction) with a constant velocity V_{gb} the following equations are satisfied:

$$-L\left(\omega(1 - mX)\frac{\partial g}{\partial \eta_1} - \kappa_o \frac{\partial^2 \eta_1}{\partial x^2}\right.$$

$$\left. + 4\mu\left(\frac{1+v}{1-v}\right)\varepsilon_0 \frac{\partial \varepsilon_0}{\partial \eta_1}(X - 2X_0X + X_0^2)\right) = -V_{gb}\frac{\partial \eta_1}{\partial x},$$

$$-L\left(\omega(1 - mX)\frac{\partial g}{\partial \eta_2} - \kappa_o \frac{\partial^2 \eta_2}{\partial x^2} + \beta\left(\frac{\partial H}{\partial \eta_2}\right)\right.$$

$$\left. + 4\mu\left(\frac{1+v}{1-v}\right)\varepsilon_0 \frac{\partial \varepsilon_0}{\partial \eta_2}(X - 2X_0X + X_0^2)^2\right) = -V_{gb}\frac{\partial \eta_2}{\partial x}. \tag{B2}$$

Multiplying $\left(\frac{\partial \eta_1}{\partial x}\right)$ in the first equation and $\left(\frac{\partial \eta_2}{\partial x}\right)$ in the second equation of Eq. (B2) and adding two equations we obtain

$$\omega(1 - mX)\left[\frac{\partial g}{\partial \eta_1} \cdot \frac{d\eta_1}{dx} + \frac{\partial g}{\partial \eta_2} \cdot \frac{\partial \eta_2}{\partial x}\right]$$

$$- \kappa_o\left[\frac{\partial^2 \eta_1}{\partial x^2} \cdot \frac{\partial \eta_1}{\partial x} + \frac{\partial^2 \eta_2}{\partial x^2} \cdot \frac{\partial \eta_2}{\partial x}\right] + \beta\frac{\partial H}{\partial \eta_2} \cdot \frac{\partial \eta_2}{\partial x}$$

$$+ 4\mu\left(\frac{1+v}{1-v}\right)\varepsilon_0(x)\left[\frac{\partial \varepsilon_0}{\partial \eta_1} \cdot \frac{\partial \eta_1}{\partial x} + \frac{\partial \varepsilon_0}{\partial \eta_2} \cdot \frac{\partial \eta_2}{\partial x}\right](X$$

$$- 2X_0X + X_0^2)$$

$$= \frac{V_{gb}}{L}\left[\left(\frac{\partial \eta_1}{\partial x}\right)^2 + \left(\frac{\partial \eta_2}{\partial x}\right)^2\right]. \tag{B3}$$

Therefore, we have

$$\omega(1 - mX)\left(\frac{\partial g}{\partial x}\right) - \kappa_o\left[\frac{\partial^2 \eta_1}{\partial x^2} \cdot \frac{\partial \eta_1}{dx} + \frac{\partial^2 \eta_2}{\partial x^2} \cdot \frac{\partial \eta_2}{\partial x}\right]$$

$$+ \beta\frac{\partial H}{\partial \eta_2} \cdot \frac{\partial \eta_2}{\partial x} + 4\mu\left(\frac{1+v}{1-v}\right)\varepsilon_0(x)\left(\frac{\partial \varepsilon_0}{\partial x}\right)$$

$$\times (X - 2X_0X + X_0^2)$$

$$= \frac{V_{gb}}{L}\left[\left(\frac{\partial \eta_1}{\partial x}\right)^2 + \left(\frac{\partial \eta_2}{\partial x}\right)^2\right]. \tag{B4}$$

Integrating both sides of the equation with respect to x the equation becomes

$$-m\omega \int_{-\infty}^{+\infty} X\left(\frac{\partial g}{\partial x}\right)dx - \kappa_o \int_{-\infty}^{+\infty}\left[\frac{\partial^2 \eta_1}{\partial x^2} \cdot \frac{\partial \eta_1}{\partial x} + \frac{\partial^2 \eta_2}{\partial x^2} \cdot \frac{\partial \eta_2}{\partial x}\right]dx$$

$$+ \beta \int_{-\infty}^{+\infty} \frac{\partial H}{\partial x}dx + 4\mu\left(\frac{1+v}{1-v}\right)\int_{-\infty}^{+\infty}\varepsilon_0\left(\frac{\partial \varepsilon_0}{\partial x}\right)$$

$$\times (X - 2X_0 X + X_0^2) dx$$
$$= \frac{V_{gb}}{L} \int_{-\infty}^{+\infty} \left[\left(\frac{\partial \eta_1}{\partial x}\right)^2 + \left(\frac{\partial \eta_2}{\partial x}\right)^2 \right] dx. \tag{B5}$$

Applying the integration $\int_{-\infty}^{+\infty} [\frac{\partial^2 \eta_1}{\partial x^2} \cdot \frac{\partial \eta_1}{\partial x} + \frac{\partial^2 \eta_2}{\partial x^2} \cdot \frac{\partial \eta_2}{\partial x}] dx = 0$ and $\int_{-\infty}^{+\infty} \frac{\partial H}{\partial x} dx = 1$ and the following approximation with an equilibrium order parameter assumption:

$$\kappa_o \int_{-\infty}^{+\infty} \left[\left(\frac{\partial \eta_1}{\partial x}\right)^2 + \left(\frac{\partial \eta_2}{\partial x}\right)^2 \right] dx \approx \sigma_{gb}, \tag{B6}$$

where σ_{gb} is the grain boundary energy, to Eq. (B5) we obtain the relation:

$$V_{gb} = M_0 \left[\beta - m\omega \int_{-\infty}^{+\infty} X \left(\frac{\partial g}{\partial x}\right) dx \right.$$
$$\left. + 4\mu \left(\frac{1+v}{1-v}\right) \int_{-\infty}^{+\infty} \varepsilon_0 \left(\frac{\partial \varepsilon_0}{\partial x}\right) (X - 2X_0 X + X_0^2) dx \right], \tag{B7}$$

where M_0 is the intrinsic mobility of the grain boundary motion and is defined as $L\kappa_o/\sigma_{gb}$ as discussed above. We can readily induce expression of the drag force if we compare Eq. (B7) with Eq. (28). Hence, the drag force is given by

$$P_{drag} = m\omega \int_{-\infty}^{+\infty} X \left(\frac{\partial g}{\partial x}\right) dx$$
$$- 4\mu \left(\frac{1+v}{1-v}\right) \int_{-\infty}^{+\infty} \varepsilon_0 \left(\frac{\partial \varepsilon_0}{\partial x}\right) (X - 2X_0 X + X_0^2) dx. \tag{B8}$$

Moreover, if we assume that ε_0 is symmetrical across the grain boundary, the drag force expression becomes simpler as

$$P_{drag} = m\omega \int_{-\infty}^{+\infty} X \left(\frac{\partial g}{\partial x}\right) dx$$
$$- 4(1 - 2X_0)\mu \left(\frac{1+v}{1-v}\right) \int_{-\infty}^{+\infty} \varepsilon_0 \left(\frac{\partial \varepsilon_0}{\partial x}\right) dx, \tag{B9}$$

since the integration $\int_{-\infty}^{+\infty} \varepsilon_0 \left(\frac{\partial \varepsilon_0}{\partial x}\right) dx$ is equal to zero.

Following a similar procedure to that discussed in Kim and Park [46], the Cahn–Hilliard equation (Eq. (22)) in a one-dimensional system with an isotropic elastic modulus approximation is employed as another expression of drag force. The Cahn–Hilliard equation becomes

$$\frac{\partial X}{\partial t} = \frac{\partial}{\partial x} \left(M_c \frac{\partial}{\partial x} \left(\frac{\partial f_{chem}}{\partial X} - m \cdot \omega \cdot g + 2\mu \left(\frac{1+v}{1-v}\right) \varepsilon_0^2 (1 - 2X_0) \right. \right.$$
$$\left. \left. - \kappa_c \frac{\partial^2 X}{\partial x^2} \right) \right). \tag{B10}$$

With a grain boundary moving at a constant velocity V_{gb} the following relation is satisfied:

$$\frac{\partial}{\partial x} \left(M_c \frac{\partial}{\partial x} \left(\frac{\partial f_{chem}}{\partial X} - m \cdot \omega \cdot g + 2\mu \left(\frac{1+v}{1-v}\right) \varepsilon_0^2 (1 - 2X_0) \right. \right.$$
$$\left. \left. - \kappa_c \frac{\partial^2 X}{\partial x^2} \right) \right) = -V_{gb} \left(\frac{dX}{dx}\right). \tag{B11}$$

Integrating both sides with respect to x we have

$$M_c \left(\frac{\partial}{\partial x} \left(\frac{\partial f_{chem}}{\partial X}\right) - m \cdot \omega \cdot \left(\frac{\partial g}{\partial x}\right) + 4\mu \frac{1+v}{1-v} (1 - 2X_0) \varepsilon_0 \frac{\partial \varepsilon_0}{\partial x} \right.$$
$$\left. - \kappa_c \frac{\partial^3 X}{\partial x^3} \right) = -V_{gb}(X - X_m). \tag{B12}$$

Rearranging Eq. (B12) using Eq. (26) we obtain

$$m \cdot \omega \cdot \left(\frac{\partial g}{\partial x}\right) = \frac{RTV_{gb}}{D} \frac{(X - X_m)}{X(1 - X)} + \frac{\partial}{\partial x} \left(\frac{\partial f_{chem}}{\partial X}\right)$$
$$+ 4\mu \left(\frac{1+v}{1-v}\right) (1 - 2X_0) \varepsilon_0 \left(\frac{\partial \varepsilon_0}{\partial x}\right) - \kappa \frac{\partial^3 X}{\partial x^3}. \tag{B13}$$

Plugging Eq. (B13) into Eq. (B9) the drag force becomes

$$P_{drag} = m\omega \int_{-\infty}^{+\infty} X \left(\frac{\partial g}{\partial x}\right) dx$$
$$- 4(1 - 2X_0)\mu \frac{1+v}{1-v} \int_{-\infty}^{+\infty} X \cdot \varepsilon_0 \left(\frac{\partial \varepsilon_0}{\partial x}\right) dx$$
$$= RTV_{gb} \int_{-\infty}^{+\infty} \frac{(X - X_m)}{D(1 - X)} dx + \int_{-\infty}^{+\infty} X \frac{\partial}{\partial x} \left(\frac{\partial f_{chem}}{\partial X}\right) dx$$
$$+ 4(1 - 2X_0)\mu \left(\frac{1+v}{1-v}\right) \int_{-\infty}^{+\infty} X \cdot \varepsilon_0 \left(\frac{\partial \varepsilon_0}{\partial x}\right) dx$$
$$- \kappa_c \int_{-\infty}^{+\infty} X \left(\frac{\partial^3 X}{\partial x^3}\right) dx$$
$$- 4(1 - 2X_0)\mu \left(\frac{1+v}{1-v}\right) \int_{-\infty}^{+\infty} X \cdot \varepsilon \left(\frac{\partial \varepsilon_0}{\partial x}\right) dx. \tag{B14}$$

Applying the integrations $\int_{-\infty}^{+\infty} X \frac{\partial}{\partial x} \left(\frac{\partial f_{chem}}{\partial X}\right) dx = 0$ and $\int_{-\infty}^{+\infty} X \left(\frac{\partial^3 X}{\partial x^3}\right) dx = 0$ the following expression is obtained:

$$P_{drag} = RTV_{gb} \int_{-\infty}^{+\infty} \frac{(X - X_m)}{D(1 - X)} dx. \tag{B15}$$

References

[1] Cahn JW. Acta Metall 1962;10:789.
[2] Lücke K, Detert K. Acta Metall 1957;5:628.
[3] Briant CL, Taub AI. Acta Metall 1988;36:2761.
[4] Kinoshita T, Munekawa S, Tanaka S-I. Acta Mater 1997;45:801.
[5] Kim JC, Heo NH, Na JG, Na JS, Woo JS, Kim GM. Scripta Mater 1998;7:1071.
[6] Heatherly L, George EP. Acta Mater 2001;49:289.
[7] Misra RDK. Surf Interface Anal 2001;31:509.
[8] Chiu YL, Ngan AHW. Metall Mater Trans A 2000;31A:3179.
[9] Millett PC, Selvam RP, Saxena A. Acta Mater 2006;54:297.
[10] Millett PC, Selvam RP, Saxena A. Acta Mater 2007;55:2329.
[11] Detor AJ, Schuh CA. Acta Mater 2007;55:4221.
[12] Trelewicz JR, Schuh CA. Phys Rev B 2009;79:094112.
[13] Johnson WC. Metall Mater Trans A 1977;8A:1413.
[14] Seah MP. J Phys F Metal Phys 1980;10:1043.
[15] Wynblatt P. J Eur Cer Soc 2003;23:2841.

[16] Tingdong X, Buyuan C. Prog Mater Sci 2004;49:109.
[17] Wynblatt P, Chatain D. Metall Mater Trans A 2006;37A:2595.
[18] Lejcek P, Hofmann S. Crit Rev Solid State Mater Sci 2008;33:133.
[19] Chapman MAV, Faulkner RG. Acta Metall 1983;31:677.
[20] Waite NC, Faulkner RG. J Mater Sci 1990;25:649.
[21] Jiang H, Faulkner RG. Acta Mater 1996;44:1857.
[22] Jiang H, Faulkner RG. Acta Mater 1996;44:1865.
[23] Sorokin MV, Ryazanov AI. J Nucl Mater 2006;357:82.
[24] Wynblatt P, Shi Z. J Mater Sci 2005;40:2765.
[25] Liu X-Y, Xu W, Foiles SM, Adams JB. Appl Phys Lett 1998;72:1578.
[26] Zhang Y, Lu G-H, Wang T, Deng S, Shu X, Kohyama M, et al. J Phys Condens Matter 2006;18:5121.
[27] Purohit Y, Jang S, Irving DL, Padgett CW, Scattergood RO, Brenner DW. Mater Sci Eng A 2008;493:97.
[28] Gottstein G, Shvindlerman LS. Grain boundary migration in metals: thermodynamics, kinetics, applications. Boca Raton, FL: CRC Press; 1999.
[29] Lücke K, Stüwe HP. Acta Metall 1971;19:1087.
[30] Hillert M, Sundman B. Acta Metall 1976;24:731.
[31] Hillert M, Odqvist J, Agren J. Scripta Mater 2001;45:221.
[32] Hillert M. Acta Mater 2004;52:5289.
[33] Hillert M. Acta Mater 1999;47:4481.
[34] Mendelev MI, Srolovitz DJ. Acta Mater 2001;49:589.
[35] Chen L-Q. Annu Rev Mater Res 2001;32:113.
[36] Boettinger WJ, Warren JA, Beckermann C, Karma A. Annu Rev Mater Res 2002;32:163.
[37] Granasy L, Pusztai T, Börzsönyi T, Toth G, Tegze G, Warren JA, et al. J Mater Res 2006;21:309.
[38] Emmerich H. Adv Phys 2008;57:1.
[39] Moelans N, Blanpain B, Wollants P. Comput Coupl Phase Diagr Thermochem 2008;32:268.
[40] Steinbach I. Modell Simul Mater Sci Eng 2009;17:073001.
[41] Fan D, Chen SP, Chen L-Q. J Mater Res 1999;14:1113.
[42] Cha P-R, Kim SG, Yeon D-H, Yoon J-K. Acta Mater 2002;50:3817.
[43] Ma N, Dregia SA, Wang Y. Acta Mater 2003;51:3687.
[44] Strandlund H, Odqvist J, Ågren J. Comp Mater Sci 2008;44:265.
[45] Grönhagen K, Ågren J. Acta Mater 2007;55:955.
[46] Kim SG, Park YB. Acta Mater 2008;56:3739.
[47] Steinbach I, Pezzolla F. Physica D 1999;134:385.
[48] Li J, Wang J, Yang G. Acta Mater 2009;57:2108.
[49] Chen L-Q, Yang W. Phys Rev B 1994;50:15752.
[50] Cahn JW. J Chem Phys 1958;28:258.
[51] Cahn JW. In: Wilkes P, Lorimer G, editors. The mechanisms of phase transformations in crystalline solids. London: The Institute of Metals; 1969.
[52] Khachaturyan AG. Theory of structural transformations in solids. New York: John Wiley & Sons; 1983.
[53] Eshelby JD. Solid State Phys 1956;3:79.
[54] Hu SY, Chen L-Q. Acta Mater 2001;49:463.
[55] Chen L-Q. In: Turchi PEA, Gonis A, editors. Phase transformations and evolution in materials. Warrendale, PA: TMS; 2000.
[56] Cahn JW. Acta Metall 1961;9:795.
[57] Allen SM, Cahn JW. Acta Metall 1979;27:1085.
[58] Zhu J, Chen L-Q, Shen J, Tikare V. Phys Rev E 1999;60:3564.
[59] Chen L-Q, Shen J. Comp Phys Commun 1998;108:147.
[60] Slater JC. J Chem Phys 1964;41:3199.
[61] Fan D, Chen L-Q. Phil Mag Lett 1997;75:187.